



JGR Space Physics

DATA ARTICLE

10.1029/2022JA030955

Key Points:

- A monthly mean global three-dimensional ionospheric electron density reanalysis data set has been obtained over one solar cycle time series.
- The data assimilation data set agrees well with the multiple independent ground- and space-based measurements
- The current data set is useful to study the spatial-temporal variations in ionospheric states from seasons to decades

Correspondence to:

X. Yue, yuexinan@mail.iggcas.ac.cn

Citation:

He, J., Yue, X., Astafyeva, E., Le, H., Ren, Z., Pedatella, N. M., et al. (2022). Global gridded ionospheric electron density derivation during 2006–2016 by assimilating COSMIC TEC and its validation. *Journal of Geophysical Research: Space Physics*, 127, e2022JA030955. https://doi.org/10.1029/2022JA030955

Received 25 AUG 2022 Accepted 8 DEC 2022

Global Gridded Ionospheric Electron Density Derivation During 2006–2016 by Assimilating COSMIC TEC and Its Validation

Jianhui He^{1,2,3,4}, Xinan Yue^{1,2,3}, Elvira Astafyeva⁴, Huijun Le^{1,2,3}, Zhipeng Ren^{1,2,3}, Nicholas M. Pedatella^{5,6}, Feng Ding^{1,2,3}, and Yong Wei^{1,2,3}

¹Key Laboratory of Earth and Planetary Physics, Institute of Geology and Geophysics, Chinese Academy of Sciences, Beijing, China, ²College of Earth and Planetary Sciences, University of Chinese Academy of Sciences, Beijing, China, ³Beijing National Observatory of Space Environment, Institute of Geology and Geophysics, Chinese Academy of Sciences, Beijing, China, ⁴CNRS UMR 7154, Institut de Physique du Globe de Paris (IPGP), Université Paris Cité, Paris, France, ⁵High Altitude Observatory, National Center for Atmospheric Research, Boulder, CO, USA, ⁶COSMIC Program Office, University Corporation for Atmospheric Research, Boulder, CO, USA

Abstract The long-term accurate specification of the Earth's ionospheric states is crucial to scientific research and applications in the space weather community. In the current work, a global monthly mean three-dimensional (3-D) ionospheric electron density product has been obtained during one solar cycle from 2006 to 2016. Specifically, an accurate 3-D product is reconstructed monthly by assimilating the Constellation Observing System for Meteorology, Ionosphere and Climate slant total electron content (TEC) into an empirical background model via the Kalman filter data assimilation algorithm. The outputs of the results have spatial resolutions of 2° in latitude, 5° in longitude, and 20 km in height, and temporal resolution of 1 hr in universal time. The accuracy and reliability of the results are systematically validated by the critical frequency at the F2 layer from global ionosonde stations, the in situ electron density from the CHAllenging Minisatellite Payload Planar Langmuir Probe, the TEC from the Massachusetts Institute of Technology, and Gravity Recovery and Climate Experiment. We found that the products agree well with the independent observations. Some well-known ionospheric climatological patterns, including the solar and seasonal variation, annual asymmetry, the Weddell Sea Anomaly, and the longitudinal wave structure, can be well illustrated. The advantages of the products are its 3-D and gridded electron density and continuous one solar cycle time series (2006–2016). It is useful to study the spatial-temporal variations in ionospheric states from seasons to decades, which can also be used as the background parameters for atmospheric and ionospheric-related scientific research and applications.

Plain Language Summary As the most successful radio occultation mission to date, Constellation Observing System for Meteorology, Ionosphere and Climate (COSMIC) has accumulated a great number of ionosphere observations during the years of 2006–2020, associated with good spatial and temporal coverage. Therefore, assimilating the COSMIC slant total electron content is a good way to get an accurate gridded state of ionosphere electron density over a long-term period. In the current work, we combine the massive accumulated COSMIC data set and our developed data assimilation algorithm to obtain the monthly mean global three-dimensional ionospheric electron density over one solar cycle (2006–2016). The data assimilation results have been validated by multiple independent ground- and space-based measurements. The current data set can be well used to capture the common climatological pattern of the spatial and temporal ionospheric variations from seasons to decades.

1. Introduction

Accurately imaging and modeling the spatial-temporal variation of Earth's ionospheric states (e.g., total electron content—TEC and electron density) is crucial to the current space weather community, as it can significantly affect radio wave propagation and many modern technological systems, such as radar telescopes, Wide Area Augmentation System, and Global Navigation Satellite System (GNSS) positioning (Jakowski et al., 2012; Yeh & Liu, 1982). In the past decade, there exists much ground- and space-based ionospheric monitoring systems, particularly radio detection equipment, developed rapidly around the world. Ground-based networks are generally located in the territory, including GNSS receivers, ionosondes and incoherent scatter radars (Mannucci et al., 2005; Reinisch & Galkin, 2011; Zhang & Holt, 2004). The ocean and polar regions cannot be well covered

© 2022. American Geophysical Union. All Rights Reserved.

HE ET AL. 1 of 17

by these types of observations. However, as an important part of the ionosphere, the equatorial ionization anomaly (EIA) is mainly distributed in the low-latitude ocean area. In situ space-based measurements can make up for the limited coverage of ground-based observations over the oceans. However, this type of observation is still insufficient to estimate the ionospheric states at all times and locations. Thus, accurately specifying the spatial-temporal variation of the ionosphere globally from direct measurement is still challenging.

Based on historical ionosphere measurements, some well-established ionosphere empirical models have been built to specify the three-dimensional (3-D) electron density. The empirical models include the International Reference Ionosphere (IRI) model, and the NeQuick model (Bilitza, 2001; Nava et al., 2008), which did not rely on the first principles of physics but on mathematical functions fit to historical ionospheric observations. In general, these models can make a relatively accurate representation of the climatological features and regular variability of the global 3-D ionospheric states, including electron density, ion densities, electron temperatures, etc. Thus, they can be easy to use for assessment and prediction purposes. However, the empirical models exhibit significant deviation from the real-world observations, especially during geomagnetic storms. Additionally, they are often inaccurate in representing the state of the ionosphere if it exhibits behavior not previously seen in observations. For example, Yue et al. (2012) found that an obvious overestimation of the low-latitude ionospheric F region densities occurred in the IRI model during the 23/24 solar minimum which was characterized by much lower densities than previous solar minima.

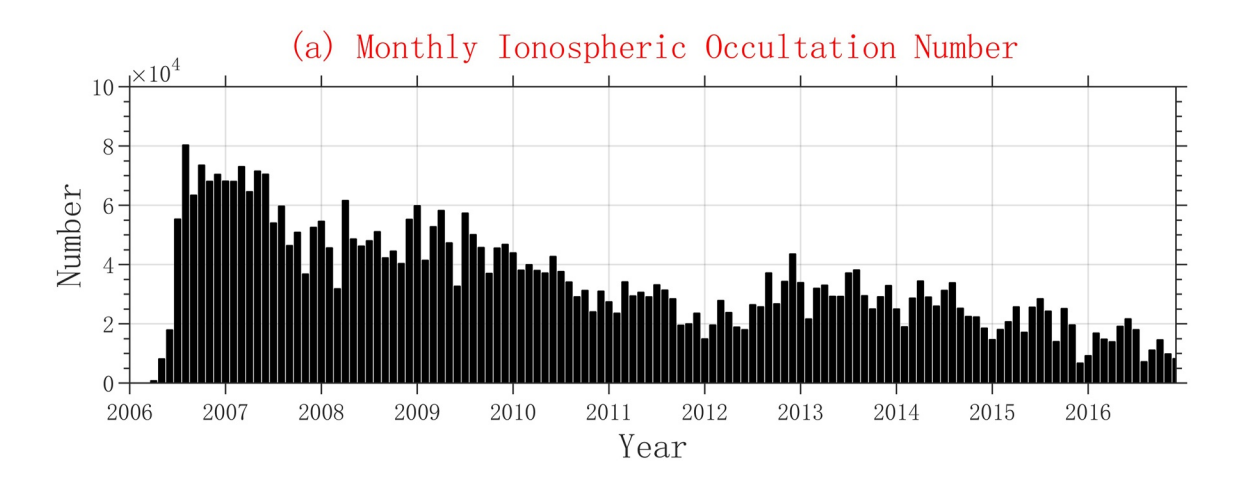
Lots of previous works have proven that the bias of the background model from observations can be further reduced to some extent by assimilating a large number of ground-based or space-based ionosphere observations (Aa et al., 2015, 2022; Galkin et al., 2012; Gardner et al., 2014; He et al., 2022; Hsu et al., 2018; Matsuo & Araujo-Pradere, 2011; Pedatella et al., 2021; Yue et al., 2012). Some mature data assimilation systems have been developed around the world for operational purposes in near real-time, such as the Ionosphere Data Assimilation three-dimension (IDA3D), the Global Assimilation Ionospheric Measurements by Utah State University (USU/ GAIM), and the Global Assimilation of Ionospheric Measurements by the Jet Propulsion Laboratory and the University of Southern California (JPL/USU GAIM) (Bust et al., 2004; Schunk et al., 2004; Wang et al., 2004). However, specifying the spatial-temporal variation of Earth's ionospheric electron density states on longer time scales is uncommon. The reasons possibly include the required computation time and limited continuous ionosphere observations. Global atmospheric reanalysis products, such as Modern-Era Retrospective analysis for Research and Applications, version 2 (MERRA2) (Gelaro et al., 2017; Molod et al., 2015) and the European Center for Medium-Range Weather Forecasts ERA5 (Hersbach et al., 2020; Hoffmann et al., 2019), have a great influence on climate monitoring and scientific research. There is also a need for ionospheric reanalyzes, which can provide a long-term archived ionospheric data assimilation data set to better study the spatial-temporal variations in ionospheric states from seasons to decades.

Fortunately, an efficient Kalman filter (KF) data assimilation algorithm has been built by Yue et al. (2014), which used a sparse matrix method to mitigate the considerable computation and storage problems. The efficient algorithm can do fast computation on a workstation. Meanwhile, a long-term valuable data set is now available from the Formosa Satellite Mission 3/Constellation Observing System for Meteorology, Ionosphere and Climate (COSMIC). As the most successful radio occultation mission to date, COSMIC has accumulated a great number of ionosphere observations during the years of 2006–2020, the rough number is ~4,652,804 provided by the COSMIC Data Analysis and Archive Center (CDAAC). These types of observations have good spatial and temporal coverage globally (Anthes, 2011; Rocken et al., 2000; Yue et al., 2011). Thus, assimilating the COSMIC slant TEC is a good way to further reduce the bias of the background model from observations, and get an accurate gridded state of ionosphere electron density over a long-term period.

In the current work, we combine the massive accumulated COSMIC data set and our developed data assimilation algorithm to obtain the monthly mean global 3-D ionospheric electron density over one solar cycle. The electron density specification has been performed by solely assimilating COSMIC radio occultation TEC measurements during the geomagnetic quiet days. Note that the data assimilation experiments have been done without assimilating any ground-based GNSS TEC data and retrieved COSMIC electron density profiles. The selected data assimilation period is about one solar cycle, starting from June 2006 and ending in December 2016. An insufficient number of COSMIC occultation TEC measurements occurred after 2016. The monthly output of the data assimilation results is 3-D gridded ionospheric electron densities with temporal and spatial resolutions of 1 hr in universal time, 2.5° in latitude, 5° in longitude, and 20 km in altitude.

HE ET AL. 2 of 17

21699402, 2022, 12, Downloaded from https://agupubs.onlinelibrary.wiley.com/doi/10.1029/2022IA030955 by University Of Colorado Librari, Wiley Online Library on [31/07/2023]. See the Terms and Conditions



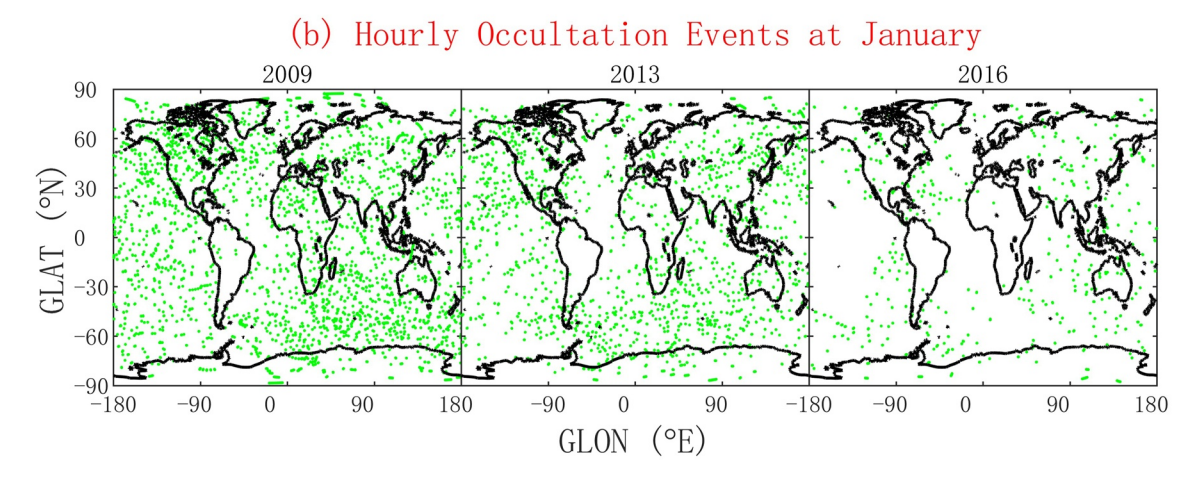


Figure 1. (a) The monthly ionospheric occultation number during a whole solar cycle from 2006 to 2016. (b) The location of the hourly occultation events at 01 universal time in January 2009, 2013, and 2016, respectively.

The electron density results are validated by independent global ionosonde stations and the CHAllenging Minisatellite Payload (CHAMP) Planar Langmuir Probe (PLP) in situ electron density measurement. In addition, the equivalent TEC is also calculated and validated by the ground-based Massachusetts Institute of Technology (MIT) vertical TEC (VTEC) and space-based Gravity Recovery and Climate Experiment (GRACE) occultation TEC data set. In addition, the reconstructed data assimilation results are also used to evaluate the capability of assimilating COSMIC data to capture the common climatological pattern of the spatial and temporal ionospheric variations.

The remainder of the paper is organized as follows. In Section 2, the data and the design of KF data assimilation experiments are described in detail. In Section 3, we present the data assimilation results. A data available statement and conclusion are given in Sections 4 and 5, respectively.

2. Data and Methods

2.1. Data Description

The level-1b absolute TECs are assimilated into an empirical ionosphere model during the years of 2006–2016, which is publicly available at the University Corporation for Atmospheric Research/COSMIC Data Analysis and Archive Center (UCAR/CDAAC, www.cosmic.ucar.edu/what-we-do/cosmic-1/data). In general, the error of occultation TEC is thought to be around 3 TECU (Yue et al., 2011). The TEC errors are mainly from the cycle slip detection, the multipath calibration, the leveling of phase to the pseudorange TEC, and the differential code bias (DCB) calibration. Figure 1 shows the monthly ionospheric occultation number and hourly occultation

HE ET AL. 3 of 17

events position distribution used in the current work. As shown in Figure 1, the top panel shows the monthly ionospheric occultation number during one whole solar cycle from 2006 to 2016. In general, the number of ionospheric occultation events has decreased from 2006 to 2016, which is due to the fact that the COSMIC satellites degraded over time, providing fewer occultations. The decrease in observations over time can also be seen in the position distribution of hourly occultation events (the bottom panel). However, the occultations locations still have even coverage around the globe within 1 month.

Apart from the assimilated COSMIC occultation TEC observations, other different types of data sets are also chosen for the independent validation purpose. The electron density results are validated by independent global ionosonde critical frequency data and the CHAMP PLP in situ electron density measurement. In addition, the equivalent assimilated TEC is also calculated, which is validated by the ground-based MIT VTEC and space-based GRACE occultation TEC data sets.

The global ionosonde critical frequency at F2 layer (foF2) measurements are from the Global Ionospheric Radio Observatory (GIRO), which can be publicly downloaded from the website (giro.uml.edu) (Reinisch & Galkin, 2011). The standard archiving output (SAO) format digisonde ionogram data were autoscaled by the Automatic Real-Time Ionogram Scaler with True height analysis (ARTIST) software to retrieve the plasma frequency. The number of available global ionosonde stations increased yearly, however, some of them did not operate continuously. During the selected data assimilation period, about 60 ionosonde stations around the world are used to make a validation with the data assimilation results.

The CHAMP was a German small satellite mission for geoscientific and atmospheric research and applications, which was managed by the Potsdam Geophysical Observatory Deutsches GeoForschungsZentrum (GFZ). This mission had a near-polar near-circular orbit with an inclination of 87.3° with about a 91 min orbit period. The orbit altitude changed from ~450 km in 2001 to ~350 km at the end of the CHAMP mission on 19 September 2010. The multifunctional and complementary payload elements, including the magnetometer, accelerometer, star sensor, GPS receiver, laser retroreflector, and ion drift meter generate several valuable data sets for atmospheric and ionospheric research and applications in weather prediction and space weather monitoring. In the current work, we use the level-2 in situ electron density measurements from the PLP (henceforth referred to as CHAMP PLP) in a low time resolution of 15 s (McNamara et al., 2007) and given in daily files during the year of 2009. The daily files are formatted as simple ASCII, which are publicly available from the website (ftp://isdcftp.gfz-potsdam.de/champ).

The MIT VTEC observations from the MIT Haystack Observatory are provided globally in a 1° by 1° bin in latitude and longitude and a 5 min time resolution (Rideout & Coster, 2006). These data are publicly available in the Madrigal Database (cedar.openmadrigal.org), which has been downloaded within the years of 2006–2016 in the current work.

The GRACE was a joint project between the National Aeronautics and Space Administration (NASA) and the Deutsches Zentrum für Luft- und Raumfahrt (DLR). Like CHAMP, the GRACE mission also had a near-circular, polar orbit (inclination: 89°) with an initial altitude of about 500 km. Due to the radio occultation payloads, the GRACE satellite mission also allows the vertical sounding of the Earth's ionosphere and neutral atmosphere (Dunn et al., 2003; Tapley et al., 2004). In this study, the occultation TEC data set from 2007 to 2014 has been used for independent validation purposes, which can be obtained from isdc. gfz-potsdam.de.

2.2. Methodology of Data Assimilation

In the current work, an empirical ionospheric model has been chosen as a background model in the data assimilation system. The empirical model was built based on the historical accumulated COSMIC ionospheric electron density profiles during the years of 2006–2020 (Le et al., 2022). The mathematical functions (Equation 1) are fitted from historical electron density data sets, which can generally represent the solar and geomagnetic activity, local time (LT), and annual, and seasonal variations. The original resolution of the reconstructed model is 10° in longitude, 2° in latitude, and 5 km in altitude.

HE ET AL. 4 of 17

The Ne_{i,j,k} stands for the electron density in the ith, jth and kth grids of the empirical model. A_{n1} , A_{n2} and A_{n3} represent the variation in solar and geomagnetic activity, the seasonal pattern, and LT, respectively. Specifically, the globe (Ne_{global}) is divided into many grids (Ne_{i,j,k}) according to longitude, latitude, and height. For each grid, we calculated values of the 21 coefficients (c_n) in Formula 1 by solving nonlinear curve-fitting problems in the least-squares sense. F107P is the mean value of daily solar radiation flux at the 10.7 cm band (F107) index and its 81 days moving average value. Kp, DOY, and LT are used here to model geomagnetic activity, day of the year, and LT variations of ionospheric electron density (Le et al., 2022).

The data assimilation algorithm is the traditional KF, which is the same as that developed by Yue et al. (2014). The efficient algorithm adopts a sparse matrix method to mitigate the storage problems of the observation operator, background error covariance, and observation error covariance. Meanwhile, an iteration linear equation method is used to deal with the large matrix inverse of the Kalman gain. Specifically, the Gaussian correlated background error covariance is assumed as previous studies, which is separable along horizontal (e.g., longitudinal and latitudinal) and vertical directions (Aa et al., 2015; Bust et al., 2004). The detailed formula can be described as,

$$P_{i,j} = C_p * x_i * x_j * e^{-\frac{\left(\log_i - \log_j\right)^2}{\left(L_{\log}\right)^2}} * e^{-\frac{\left(\ln t_i - \ln t_j\right)^2}{\left(L_{\ln}t\right)^2}} * e^{-\frac{\left(h_i - h_j\right)^2}{\left(L_h\right)^2}}$$
(2)

where $lon_{i,j}$, $lat_{i,j}$ and $h_{i,j}$ refer to the location of grid point i and j in background model. L_{lon} , L_{lat} and L_h stand for the longitudinal, latitudinal and altitude correlation length, which are 20° , 10° , and 100 km. x_i and x_j stand for the background electron density at grid point i and j. The coefficient C_p is configurable, and the typical value is 0.01.

Concerning the observation operator, it plays a key role in ingesting real-world observations into an empirical or first-principle background model. The observation operator is also called the forward model in the data assimilation community. The function of the observation operator maps the model-state vector to the model-equivalent value of the observations. The COSMIC radio occultation TEC observations stand for the integrated electron density along the raypath between GNSSs satellites (e.g., GPS) and low earth orbiting satellites (e.g., COSMIC). The observation operator of radio occultation TEC can be given as,

$$stec = \sum_{i=1}^{n} ne_i * \Delta s_i$$
 (3)

where stec is the equivalent radio occultation TEC of the background model along the GNSS raypath. ne_i and Δs_i are the electron density and the raypath length within the ith grid of the background model. Besides, to make a cross-comparison with the measurements (e.g., MIT VTEC and GRACE radio occultation TEC), the synthetic TECs from both the background model and data assimilation are also calculated by integrating 3-D gridded electron density along the raypath between receivers and GPS satellites. According to Formula (3), one can expect that the accuracy of the synthetic TECs from data assimilation is better than that from the background model if there exist accurate 3-D gridded electron density states of data assimilation results.

We notice that there exists a limited domain of the background model heights (e.g., 140–700 km). This means that the electron density is not included in the topside ionosphere and plasmasphere (e.g., >700 km). However, there is still a significant contribution to GPS slant TEC from the electron density above the upper boundary of the background model. Generally, the topside TEC could still be several TECU, which depends on the solar activity level. The COSMIC radio occultation slant TEC includes contributions from the electron density between the COSMIC receivers (around 550 km) and the GNSS satellites (around 20,000 km) when the elevation angle

HE ET AL. 5 of 17

ibrary on [31/07/2023]. See the

is negative. Thus, in the current work, Chapman-fitted function is used to extrapolate the ionosphere electron density above the model upper boundaries. Using the extrapolation method, the electron density up to around 20,000 km can be first obtained at each latitudinal and longitudinal grid of the background model. Then, the topside slant TEC contributions can be removed along each line of sight of the GPS raypath. Meanwhile, to get a comparable TEC from the background model and data assimilation with MIT VTEC and GRACE radio occultation TEC, the topside slant TEC contributions are also added to each line of sight of the GPS raypath. There are several problems with the extrapolation method. For example, the scale height changes when H⁺ becomes the dominant ion. However, this method still represents an improvement over the assumption that there is no plasma above the upper boundary of the background model.

2.3. Experimental Setup

Based on the data and method described above, the COSMIC radio occultation observations are assimilated into the empirical ionosphere background model via a KF during one whole solar cycle from 2006 to 2016. The data assimilation time window is set to be one hour in universal time. The output of the data assimilation result has a spatial resolution of 2° latitude, 5° longitude, and 20 km altitude. Note that the resolution can be flexibly adjusted. The resolution of the background model can be interpolated into the same as that of the data assimilation one. The longitudes, latitudes, and heights range from -180°E to 180°E , -80°N to 80°N , and 140 to 700 km, respectively. In addition, the ionosphere empirical model default run without conducting data assimilation is also performed during the same period, which is henceforth referred to as the control run. Both the control run and the data assimilation experiment are driven by the actual F10.7 solar flux and Kp geomagnetic indices.

3. Results

3.1. Total Electron Content Comparison

Figure 2 first gives the magnetic latitude-local time variation of vertical TEC comparison among MIT VTEC observations, control run, and data assimilation results for four different seasons in 2009. In general, the common seasonal variation can be well found in MIT VTEC observations, control, and data assimilation. The observations show a significant two-peak EIA structure at low latitudes. A stronger electron density exists in the equinox (e.g., March and September) than that in the solstice (e.g., June and December). Meanwhile, an evident annual asymmetry or December anomaly can also be found in all results, namely, with more density in the December solstice than in the June solstice. The control run, which includes the seasonal and annual effects (A_{n2} in Formula 1), can also reproduce similar seasonal and annual patterns. However, an underestimated value occurs in the low latitudes and equatorial regions, which is due to the fact that the empirical ionosphere model can generally depict the mean state of the climatological pattern. We notice that the two-peak EIA structure cannot be reproduced by the control run. For the data assimilation results, the seasonal variation pattern of data assimilation is much more consistent with the observations in comparison with the control run. In addition, the data assimilation results show an obvious two-peak EIA structure. The underestimation of VTEC can be corrected to some extent and is much closer to the observations, especially around the low-latitude and equatorial regions. Quantitatively, the averaged deviations of the control run from the MIT-VTEC are 0.88, 1.00, 1.33, and 2.06 TECU in March, June, September, and December, which are 0.43, 0.54, 0.80, and 0.34 TECU for the data assimilation result.

Figure 3 further shows VTEC comparison at a fixed 1400 LT in four different seasons of 2009. The same conclusions as found in Figure 2 can be also found in Figure 3. The value and pattern of VTEC in the empirical ionosphere background model (i.e., control) have been corrected and are in better agreement with the MIT VTEC observations after assimilating COSMIC radio occultation TEC measurements. For example, An obvious interhemispheric asymmetry of the EIA crests with a global view exists in the June and December solstices. At the selected 1400 fixed LT, for June solstices, the value of the winter crest (Southern Hemisphere) is smaller than that of the summer crest (Northern Hemisphere). However, the stronger crest shifts to the summer hemisphere (Southern Hemisphere) from the winter hemisphere (Northern Hemisphere) in December solstices. This finding is generally consistent with previous work (Huang et al., 2018; Luan et al., 2015). Again, the obvious EIA crest and trough can also be reconstructed by the data assimilation, while it is not present in the control run. Quantitatively,

HE ET AL. 6 of 17

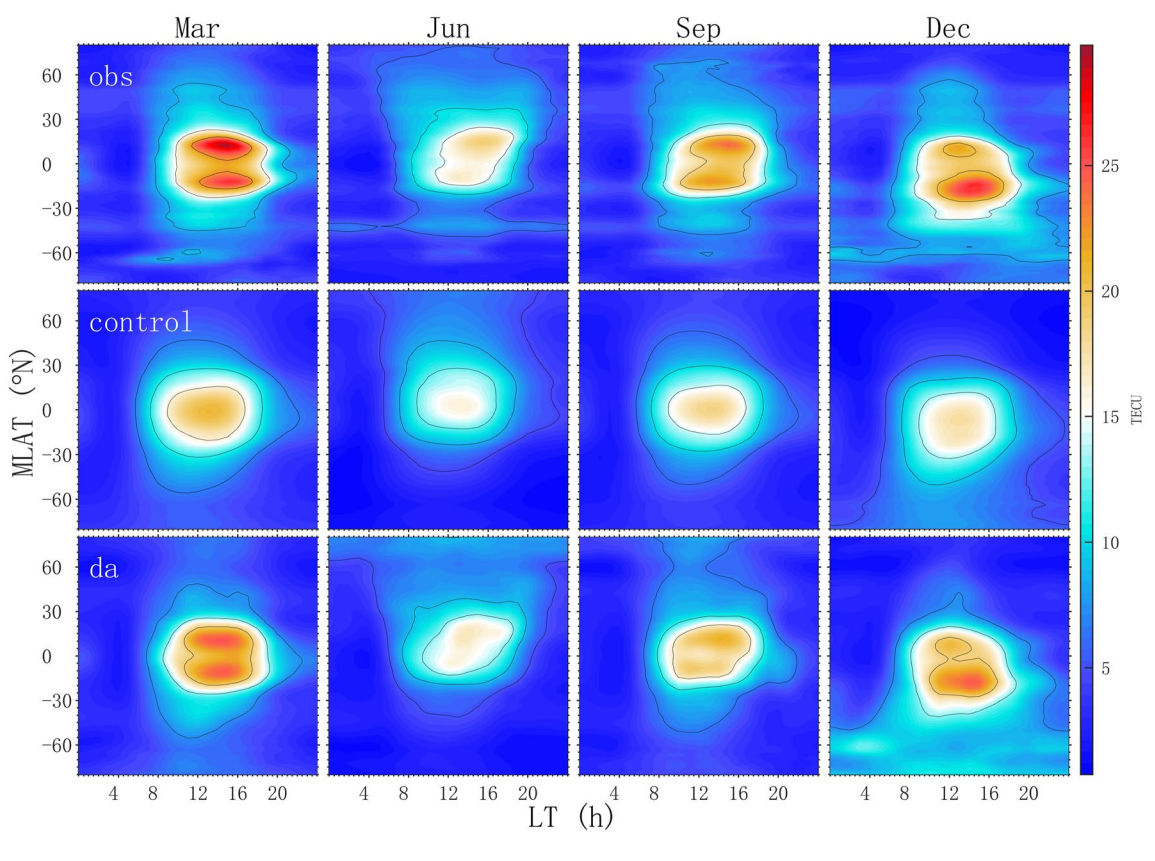


Figure 2. The seasonal magnetic latitude-local time variation of vertical TEC (VTEC) comparison among Massachusetts Institute of Technology VTEC observations, control, and the data assimilation during the year of 2009. From left to right panels stand for March, June, September, and December, respectively.

the averaged deviations of the control run from the MIT-VTEC are 2.66, 1.27, 2.62, and 3.23 TECU in March, June, September, and December, which are 0.99, 1.02, 1.62, and 0.75 TECU for the data assimilation result.

To get a statistical assessment of the improvement of ionosphere grided vertical TEC results, Figure 4 shows the root-mean-squared errors (RMSEs) comparison and the zonal mean value comparison of the global VTEC among MIT VTEC observations, control, and data assimilation during a whole solar cycle from 2006 to 2016. The solar activity F10.7 index is given in Figure 4a to represent the variations in solar radiation. From Figure 4b, obvious solar activity and seasonal variations exist in the control RMSEs. The value has an increase as the solar activity increases, and the biggest one can be up to around 10 TECU under higher solar activity. The RMSEs values of control run are still greater than that of data assimilation from 2006 to 2016. However, the solar activity and seasonal variations in data assimilation have been eliminated to some extent. It means that the value of data assimilation is much closer to the MIT VTEC in different solar activities and seasons. The zonal mean VTEC comparison can further confirm this conclusion. From Figures 4c–4e, we found that there exists more agreement in either value or pattern between data assimilation and MIT VTEC within a whole solar cycle. The overall mean deviation of data assimilation from the MIT VTEC is –0.11 TECU, which is smaller than that of the control one (2.32 TECU).

In addition to the previous ground-based vertical TEC comparison, Figure 5 gives the space-based occultation TEC comparison for the GRACE measurements, control and data assimilation during the years of 2007–2014. From Figure 5a, the correlation coefficient of occultation TEC between GRACE and control is 0.70, and 0.94 for data assimilation. Regarding the RMSEs, from Figure 5b, there still exists a smaller value of data assimilation in comparison with the control run from 2007 to 2014. The averaged RMSEs of occultation TEC with respect to the GRACE observations for the control run is 44.37, and 24.16 TECU for the data assimilation case.

As described above, the value of TEC in the empirical ionosphere background model has been improved and is much closer to the observations after assimilating COSMIC radio occultation TEC measurements. Another

HE ET AL. 7 of 17

21699402, 2022, 12, Downloaded

wiley.com/doi/10.1029/2022JA030955 by University Of Colorado Librari, Wiley Online Library on [31/07/2023]. See the Terms.

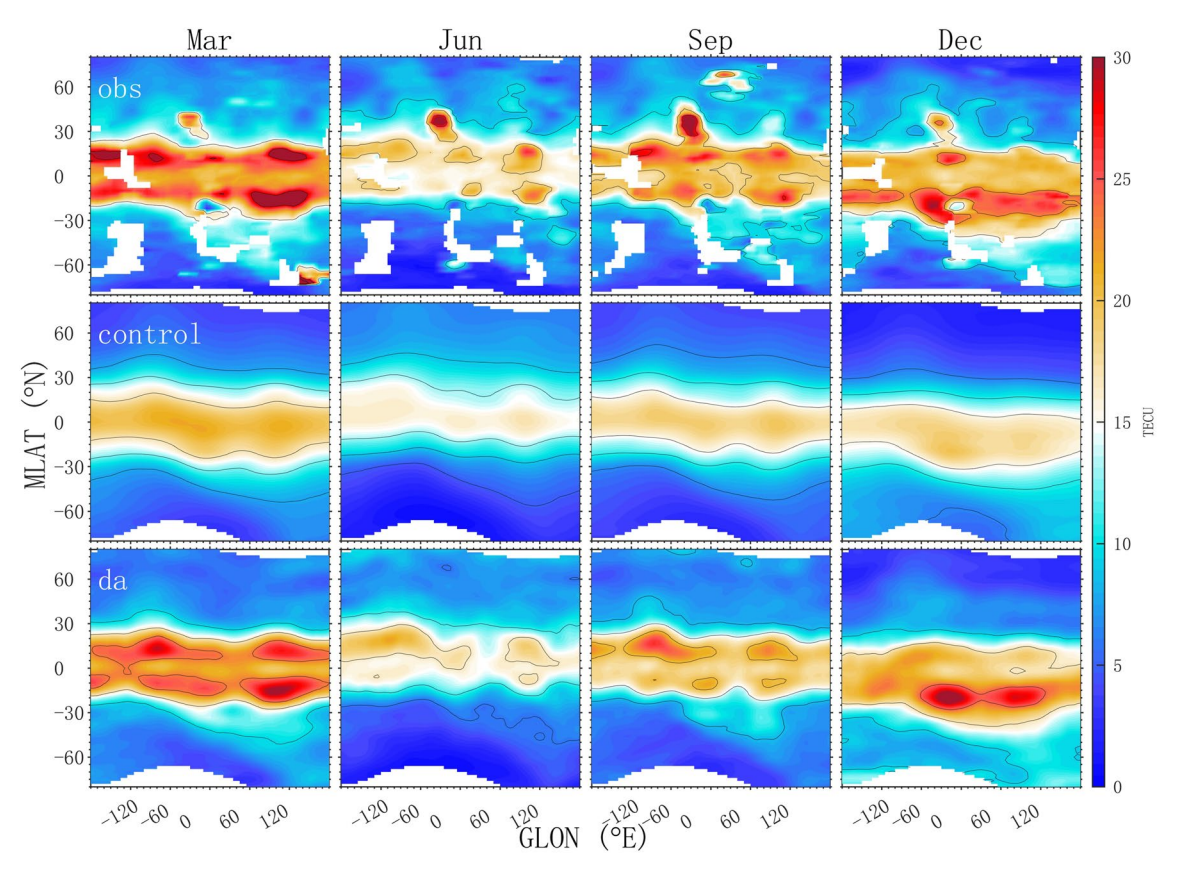


Figure 3. The seasonal longitude-magnetic latitude distribution of vertical TEC (VTEC) comparison among Massachusetts Institute of Technology VTEC observations, control, and the data assimilation at a fixed 1300–1500 local time during the year of 2009. From left to right panels stand for March, June, September, and December, respectively.

important thing is that the TEC data assimilation results can capture not only more real solar activity and seasonal variations, but also the completed structure of the EIA crest and trough at any time. For the control run, it was constructed by the historical database from COSMIC radio occultation electron density. Based on the assumption of spherical symmetry, the occultation technique would smooth the great spatial variation of electron density at the equator and low latitudes (Yue et al., 2010). The EIA structure of the control run TEC may be not clear at certain longitudes at certain times. However, for the data assimilation system, the control run is only used as a background reference. One of the most important things is that if the assimilated observations contain EIA information, then the data assimilation model will usually reflect similar results. Therefore, we can see that the assimilation results reproduce the EIA structure very well.

We notice that, from Formula 3, the GRACE radio occultation slant TECs are calculated by integrating 3-D gridded electron density along the raypath between GRACE receivers and GNSS satellites when the elevation angle is negative. Compared with the control run, the smaller RMSEs of occultation TEC for the data assimilation case indirectly reflect that an improvement of the 3-D gridded electron density has been obtained in data assimilation results. In the following sections, we will give a detailed evaluation of the accuracy of the electron density assimilation results. The ground-based ionosonde data set and space-based in situ electron density will be taken into consideration.

3.2. Ionospheric Critical Frequency at F2 Layer (foF2) Comparison

The peaked electron density at the F2 layer (NmF2) is a key parameter for ionosphere research. The NmF2 can be accurately inferred by the ionospheric critical frequency at F2 (foF2) from the ground-based ionosonde stations according to the below Formula 4. Thus, the foF2 data is useful to validate an improvement of the 3-D gridded electron density assimilation results.

HE ET AL. 8 of 17

21699402, 2022, 12, Downloaded from https://agupubs.onlinelibrary.wiley.com/doi/10.1029/2022/A039955 by University Of Colorado Librari, Wiley Online Library on [31.07/2023]. See the Terms and Conditions (https://onlinelibrary.wiley.com/terms-and-conditions) on Wiley Online Library for rules of use; OA articles

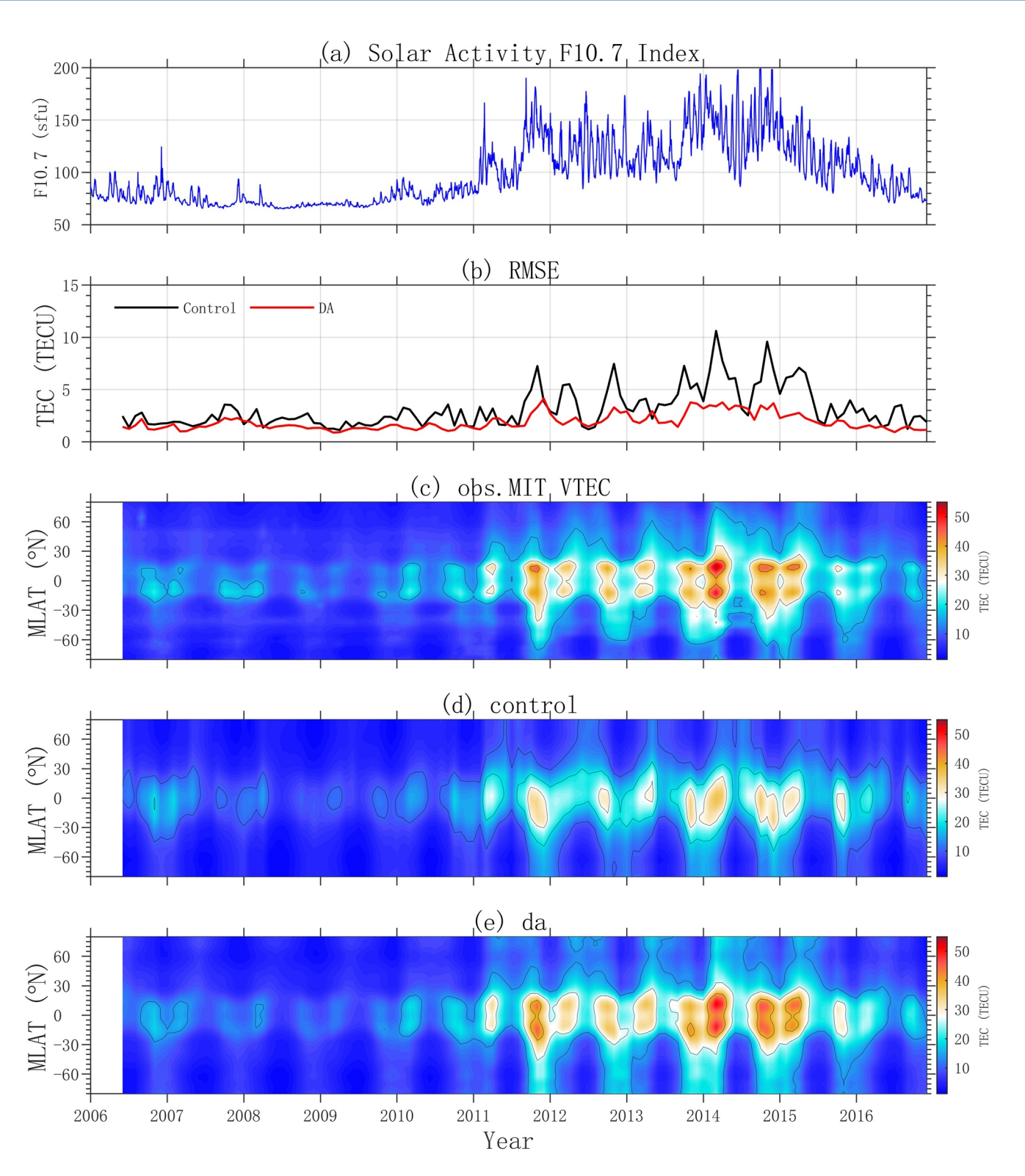


Figure 4. (a) The solar activity F10.7 index, (b) the root-mean-squared errors of global vertical TEC (VTEC) in comparison with Massachusetts Institute of Technology (MIT) VTEC for the control and data assimilation, and (c, e) the zonal mean value comparison of VTEC among MIT VTEC observations, control, and data assimilation during a whole solar cycle from 2006 to 2016.

HE ET AL. 9 of 17

/doi/10.1029/2022IA030955 by University Of Colorado Librari, Wiley Online I

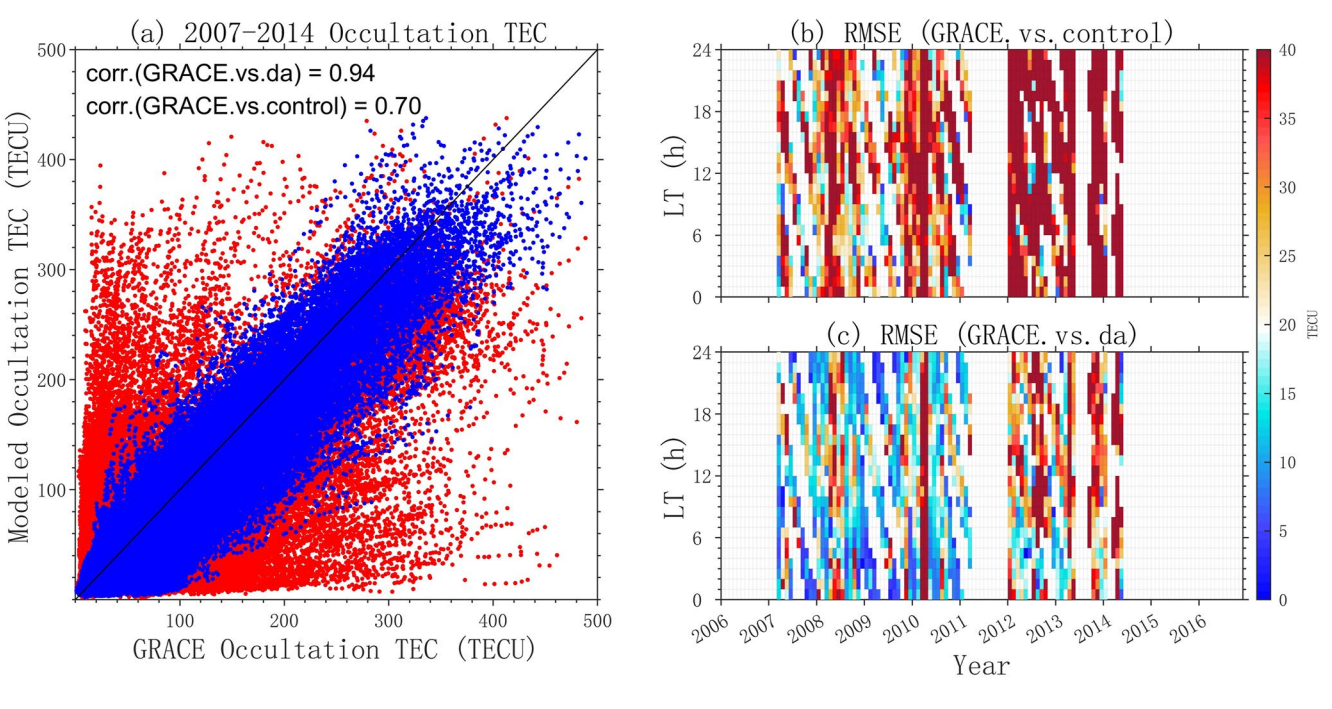


Figure 5. (a) Comparison of modeled versus observed Gravity Recovery and Climate Experiment (GRACE) occultation total electron content and (b, c) the root-mean-squared errors comparison among the GRACE measurements, control, and data assimilation during the years of 2007–2014.

$$NmF2 = [1.24 \times 10^{10} (foF2)^{2}] m^{-3}$$
(4)

The NmF2 is in el/m³ and foF2 is in MHZ.

Figure 6 shows the foF2 comparison among the global ionosonde measurements, control, and data assimilation result during the whole year of 2009 (solar low activity) and 2013 (solar high activity). We notice that the solar activity within which the foF2 data exists was sufficiently modeled by the control run, that is, the larger foF2 value at solar high activity. Besides, the control run also shows the correct LT variations. However, an overall underestimation occurred in the control run for both selected years, especially in the low-latitude and equatorial regions. For the data assimilation case, the value of underestimated foF2 can be corrected greatly and is much closer to that of the observations. Quantitatively, the foF2 RMSEs of the control run and data assimilation results from the ionosonde measurements are 0.58 and 0.41 MHZ under low solar activity (e.g., 2009), and are 1.19 and 0.60 under high solar activity (e.g., 2013).

Figure 7 compares the monthly critical frequency at the F2 layer between the ionosonde and data assimilation over different magnetic latitudes in the northern and southern hemispheres from 2006 to 2016. Similar solar activity and seasonal variations as those seen in MIT VTEC are also found in ionosonde foF2 measurements at different magnetic latitudes. Meanwhile, the value and feature of the assimilated foF2 are much more consistent with those of the observations at all LTs during the whole solar cycle. A quantitative foF2 value comparison at different magnetic latitudes is calculated. The averaged RMSEs of data assimilation foF2 from ionosonde measurements are 0.45 MHZ at 30°N magnetic latitude, and 0.47 MHZ at 30°S magnetic latitude.

Figure 8 gives the statistical results of the mean deviation and RMSEs of the control run and data assimilation from the global available ionosonde foF2 measurements during the years from 2006 to 2016. Indicated from either the mean deviation or the RMSEs, the larger deviations of the control run from the real observations occur in the low latitudes at all LTs. It is due to the fact that the empirical ionosphere model can generally depict the mean state of the climatological pattern. We found that an obvious improvement exists in the data assimilation in comparison with the control run during the nighttime and daytime. With regard to mean deviation, the errors between the control run and observation at daytime (08–20 LT) and nighttime are 0.37 and 0.45 MHZ, respectively, which are -0.03 and 0.14 MHZ for data assimilation. In terms of RMSEs, the errors between the control

HE ET AL. 10 of 17

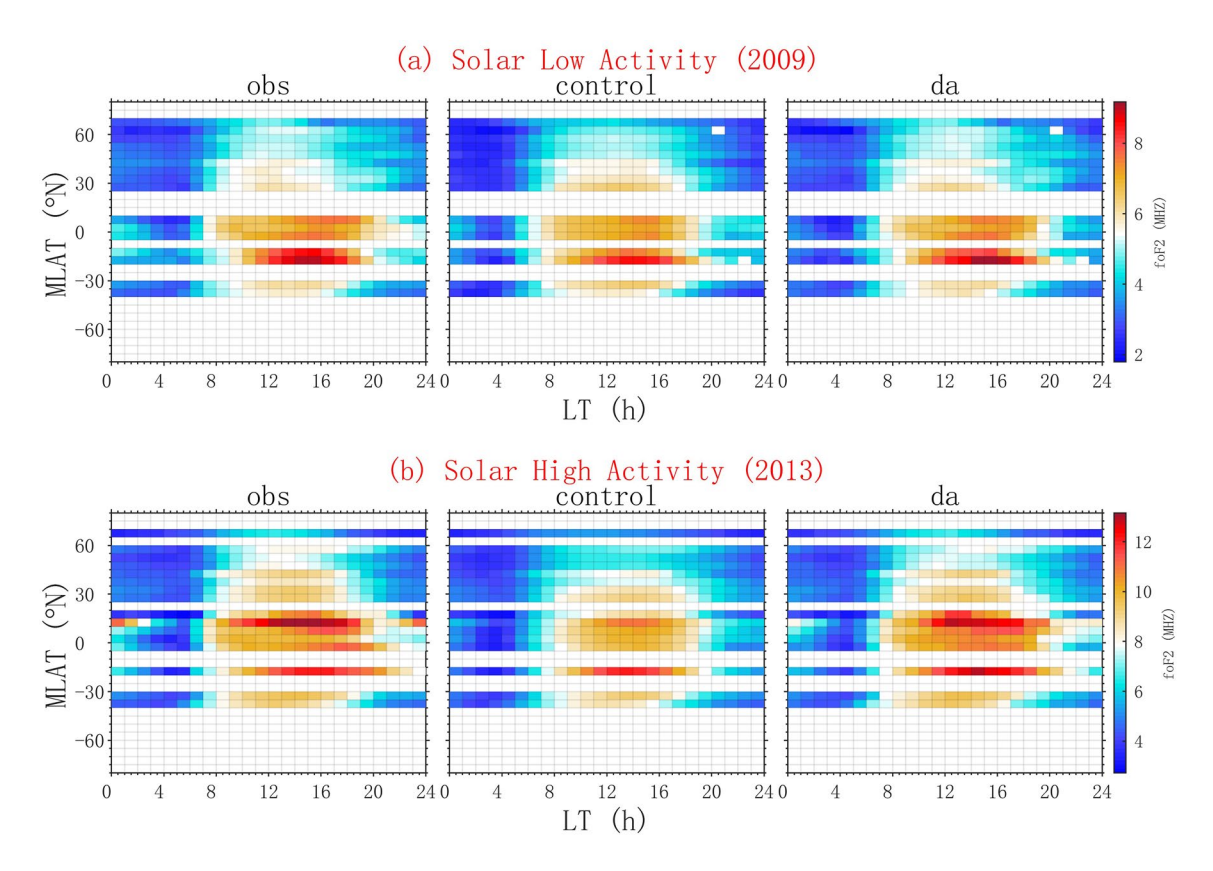


Figure 6. The magnetic latitude-local time variation of the monthly foF2 comparison among the global ionosonde measurements, control, and data assimilation result during the whole year of 2009 (a) and 2013 (b).

run and observation at daytime and nighttime are 0.77 and 0.95 MHZ, respectively, which are 0.37 and 0.56 MHZ for data assimilation.

As indicated above, one of the important ionosphere parameters, that is, NmF2, can also be obtained by assimilating COSMIC radio occultation TEC measurements. It is due to the fact that the electron density at the F2 layer accounts for the majority proportion of the TEC. According to Formula 3, one can expect a better NmF2 value and pattern of the data assimilation results relative to the climatological model, that is, control run. Besides, owing to the virtue of global spatial coverage of space-borne COSMIC TEC measurements, the data assimilation results are capable of providing the latitudinal and longitudinal structures of foF2 or NmF2 on a global scale. The completed NmF2 map is necessary for ionosphere modeling and physical mechanism research.

3.3. Electron Density Comparison

In order to get a clear knowledge of the improvement of the gridded electron density at a fixed height, Figures 9 and 10 give the dayside and nightside electron density comparison among CHAMP PLP in situ electron density measurements, control, and data assimilation results for different seasons of 2009. The heights of the CHAMP during the selected period are near 350 km. Note that due to the near-polar and near-circular orbit of the CHAMP satellite, the LT of the dayside and nightside observations varies from month to month. Thus, the dayside results are for 19, 10, 13, and 17 LT in March, June, September and December, and the nightside consists of 07, 22, 01, and 05 LT. From Figure 9, in general, the common feature as represented by CHAMP PLP in situ measurements includes the interhemispheric asymmetry feature around the June and December solstice, and an obvious wave 4 longitude structure of the EIA crest during the September equinox. According to previous studies, a stronger longitudinal wave 4 pattern occurred around August–September than in other months (Chang et al., 2013; Forbes et al., 2008; Wan et al., 2008). The same asymmetry feature and longitude structure can be well reproduced by the control run during the daytime. Besides, as shown in the observations, the control run has two peak structures of the EIA at some longitude sectors. However, the value of electron density at the selected height of 350 km is

HE ET AL. 11 of 17

21699402, 2022, 12, Downloaded

from https://agupubs.onlinelibrary.wiley.com/doi/10.1029/2022IA030955 by University Of Colorado Librari, Wiley Online Library on [31.07/2023]. See the Terms and Conditions (https://onlinelibrary.viley.com/doi/10.1029/2022IA030955 by University Of Colorado Librari, Wiley Online Library on [31.07/2023]. See the Terms and Conditions (https://onlinelibrary.viley.com/doi/10.1029/2022IA030955 by University Of Colorado Librari, Wiley Online Library on [31.07/2023]. See the Terms and Conditions (https://onlinelibrary.viley.com/doi/10.1029/2022IA030955 by University Of Colorado Librari, Wiley Online Library on [31.07/2023]. See the Terms and Conditions (https://onlinelibrary.viley.com/doi/10.1029/2022IA030955 by University Of Colorado Librari, Wiley Online Library on [31.07/2023]. See the Terms and Conditions (https://onlinelibrary.viley.com/doi/10.1029/2022IA030955 by University Of Colorado Librari, Wiley Online Library on [31.07/2023]. See the Terms and Conditions (https://onlinelibrary.viley.com/doi/10.1029/2022IA030955 by University Of Colorado Librari, Wiley Online Library on [31.07/2023]. See the Terms and Conditions (https://onlinelibrary.viley.com/doi/10.1029/2022IA030955 by University Of Colorado Librari, Wiley Online Library on [31.07/2023]. See the Terms and Conditions (https://onlinelibrary.viley.com/doi/10.1029/2022IA03095 by University Of Colorado Library.

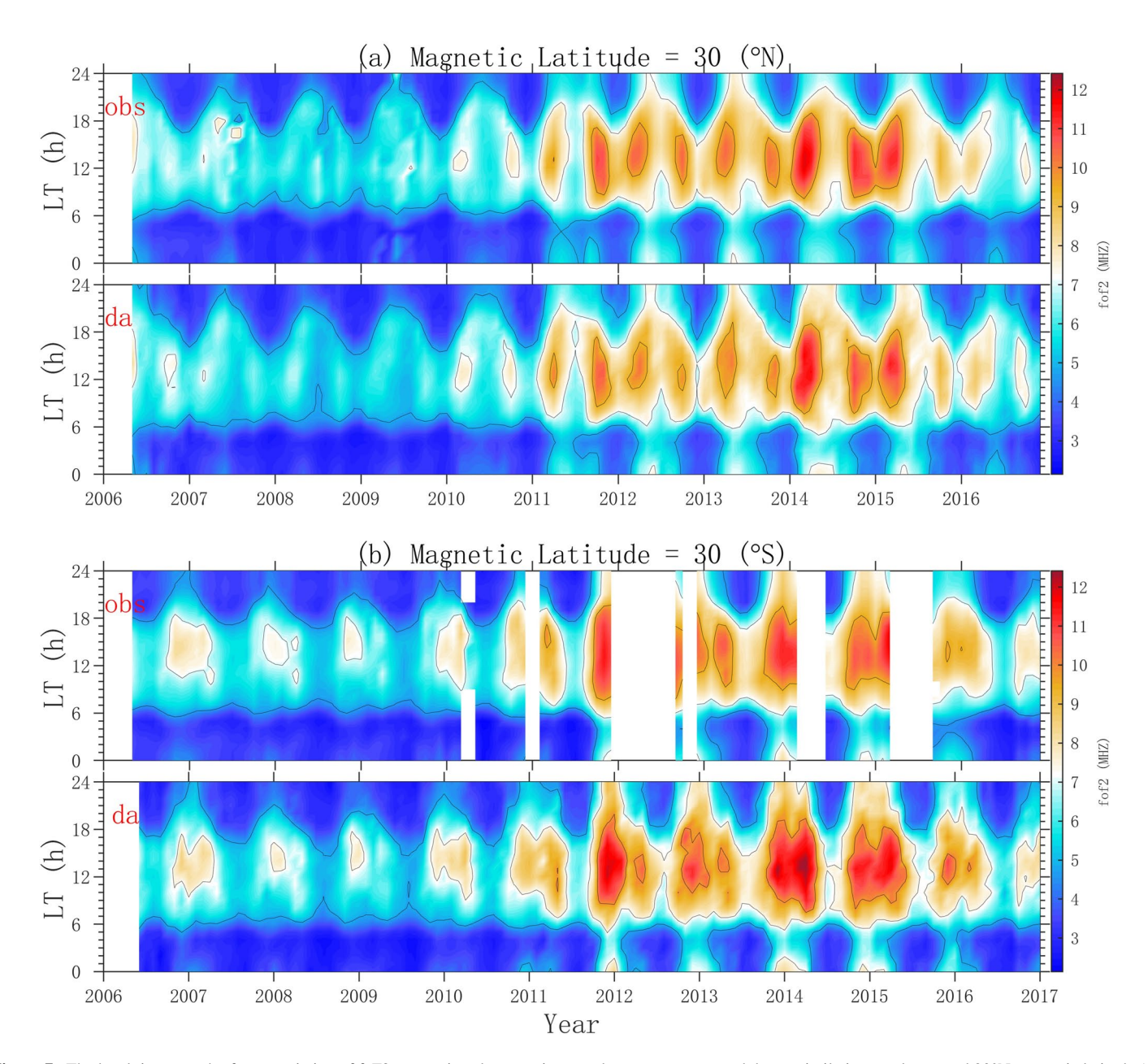


Figure 7. The local time-month of year variation of foF2 comparison between ionosonde measurements and data assimilation results around 30°N magnetic latitude (a) and 30°S magnetic latitude (b) during the years of 2006–2016.

underestimated in the control run. The value of data assimilation is much closer to that of observations in comparison with the control run.

Results for the nightside electron density comparison are also shown in Figure 10. We found that the control run can approximately capture the electron density enhancement regions in some seasons. For example, the nightside electron density enhancement occurs around the equatorial regions in March, and the northern low latitudes in June. However, a larger discrepancy occurs in September and December. The data assimilation results can well represent the feature of ionosphere electron density during the nighttime for all four seasons in comparison with the control run. Especially, an obvious Weddell Sea Anomaly (WSA) can be better reproduced by the data assimilation electron density in December. This is a type of summer ionospheric anomaly characterized by a greater nighttime ionospheric density than that in the daytime in the region near the Weddell Sea area.

HE ET AL. 12 of 17

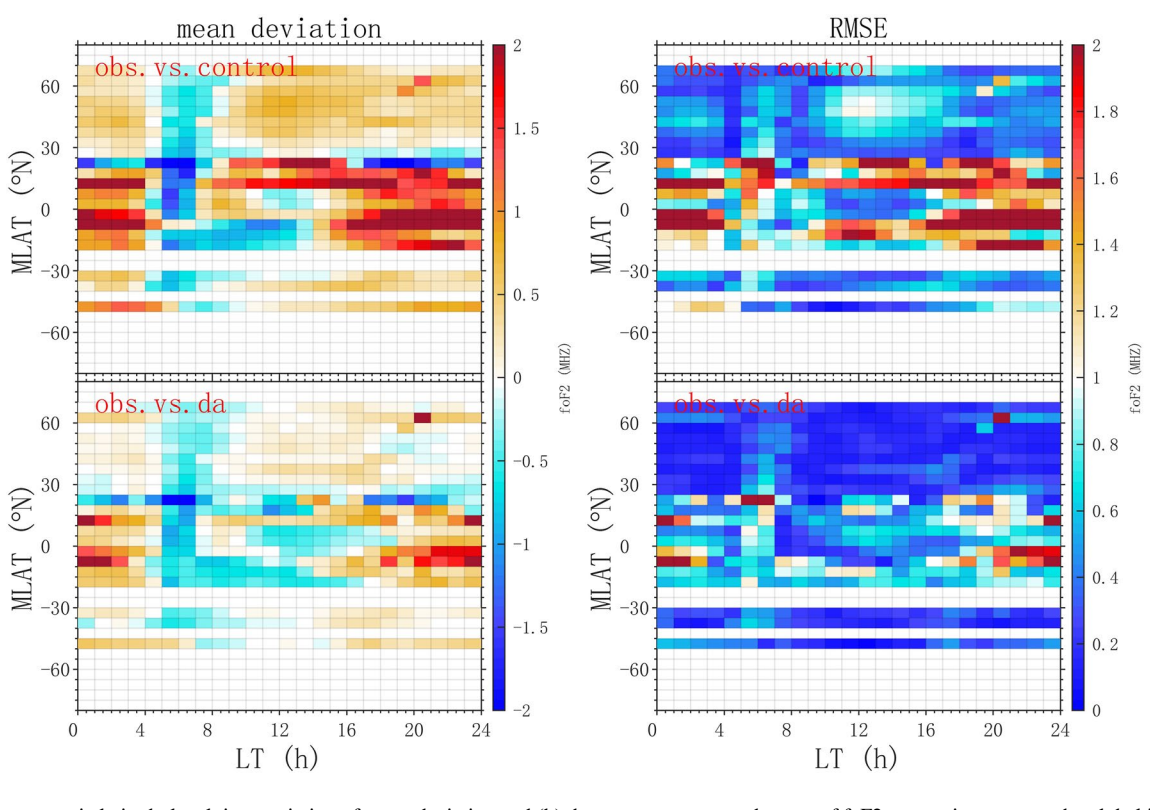


Figure 8. (a) The magnetic latitude-local time variation of mean deviation and (b) the root-mean-squared errors of foF2 comparison among the global ionosonde measurements, control, and data assimilation result during the years from 2006 to 2016.

The electron density comparison results illustrate that the electron density can be better modeled for the control run during the daytime than during the nighttime. One possible explanation is that the mathematical functions are not well fitted during the nighttime due to the lower background ionosphere electron density. In addition, owing to assimilating the COSMIC observations, a better specification of the gridded electron density during both the daytime and the nighttime can be obtained.

To further illustrate the accuracy of the reconstructed 3-D electron density profiles, Figure 11 shows the altitude—magnetic latitude variation of electron density profiles comparison among COSMIC retrieved electron density profiles measurements, control, and the data assimilation result at 45°E approximately 1300 LT during June for each year between 2007 and 2015. From the observations, the value of the winter EIA crest (the Southern Hemisphere) is stronger than that of the summer EIA crest (the Northern Hemisphere) at the selected 1300 LT at the June solstice. A similar feature can also be reproduced during the years of 2007–2009 in our empirical background model. However, the feature cannot be well reproduced by the control run during the years of 2011–2015, especially in the southern crest. Generally, the control run stands for the climatological mean states, and the EIA structure may be not correct at certain longitudes at certain times. Another reason is that the mathematical functions are likely not well fitted by the decreased radio occultation observations during the years of 2011–2015. For the data assimilation results, both the features and the value of the EIA crest are consistent with the COSMIC electron density profiles measurements. The RMSEs of control run from observations are 6.09 * 10⁴ el/cm³ and 1.25 * 10⁵ el/cm³ in the year of 2009 (solar low activity) and 2013 (solar high activity), and are 6.07 * 10⁴ and 1.06 * 10⁵ el/cm³ for data assimilation.

The electron density profiles comparison results again demonstrate that assimilating the radio occultation TEC observations into the climatological ionosphere model is necessary to better specify the whole electron density profiles. The data assimilation results further provide an opportunity to capture the accurate EIA structure and the time evolution of that, that is, the pattern of interhemispheric asymmetry of the EIA crest. Huang et al. (2018) indicated both photochemical processes and transequatorial neutral wind transportation could contribute to the asymmetry of EIA around solstices. Therefore, accurate electron density profiles are useful for low latitude and equatorial ionosphere research.

HE ET AL. 13 of 17

21699402, 2022, 12, Downloaded from https://agupubs.onlinelibrary.wiley.com/doi/10.1029/2022IA030955 by University Of Colorado Librari, Wiley Online Library on [31.07/2023]. See the Terms and Conditions (https://onlinelibrary.wiley

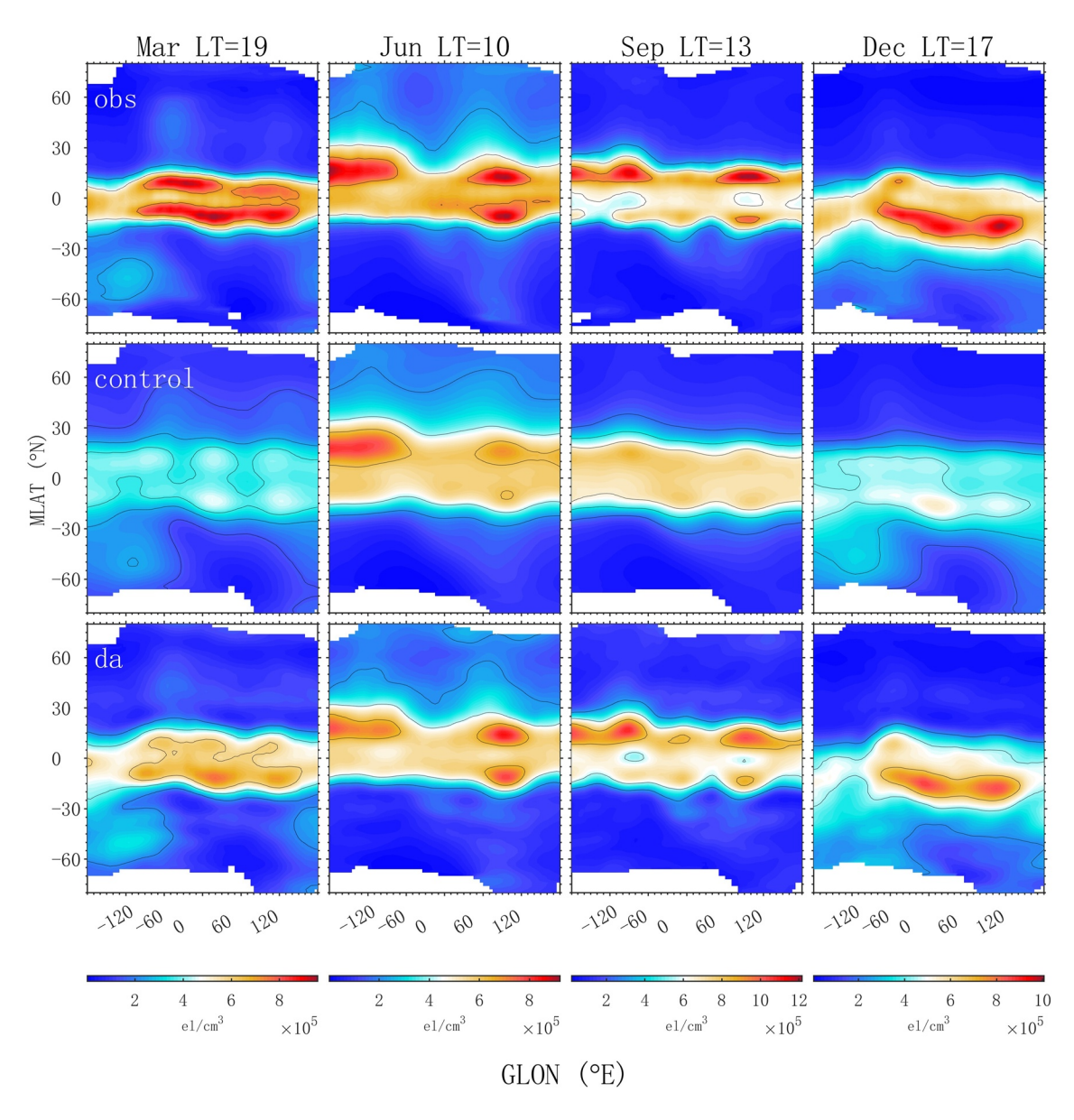


Figure 9. The longitude-magnetic latitude distribution of dayside electron density comparison among CHAllenging Minisatellite Payload Planar Langmuir Probe electron density measurements, control, and data assimilation result around 350 km at different seasons during the year of 2009. From the left panels to the right panels represent the comparison results at 19, 10, 13, and 17 LT in March, June, September, and December, respectively.

Generally, the COSMIC radio occultation TEC cannot be directly used to investigate the ionosphere variations, which is due to the fact that this type of data stands for the integrating electron density along the raypath. However, in the current work, we provide a reliable 3-D electron density data set based on the assimilation of the COSMIC radio occultation TEC measurements over one solar cycle time series. Compared with the traditional ionosphere climatological model, the data assimilation results can provide a more real common ionospheric pattern, such as the solar and seasonal variation, annual asymmetry and the WSA. Besides, the data assimilation results can also provide global coverage of the ionosphere key parameters, such as the TEC, NmF2 and electron density profiles, which can well capture the time evolution structure of the completed EIA around the low-latitude regions.

HE ET AL. 14 of 17

21699402, 2022, 12, Downloaded

from https://agupubs.onlinelibrary.wiley.com/doi/10.1029/2022IA030955 by University Of Colorado Librari, Wiley Online Library on [31.07/2023]. See the Terms and Conditions (https://onlinelibrary.viley.com/doi/10.1029/2022IA030955 by University Of Colorado Librari, Wiley Online Library on [31.07/2023]. See the Terms and Conditions (https://onlinelibrary.viley.com/doi/10.1029/2022IA030955 by University Of Colorado Librari, Wiley Online Library on [31.07/2023]. See the Terms and Conditions (https://onlinelibrary.viley.com/doi/10.1029/2022IA030955 by University Of Colorado Librari, Wiley Online Library on [31.07/2023]. See the Terms and Conditions (https://onlinelibrary.viley.com/doi/10.1029/2022IA030955 by University Of Colorado Librari, Wiley Online Library on [31.07/2023]. See the Terms and Conditions (https://onlinelibrary.viley.com/doi/10.1029/2022IA030955 by University Of Colorado Librari, Wiley Online Library on [31.07/2023]. See the Terms and Conditions (https://onlinelibrary.viley.com/doi/10.1029/2022IA030955 by University Of Colorado Librari, Wiley Online Library on [31.07/2023]. See the Terms and Conditions (https://onlinelibrary.viley.com/doi/10.1029/2022IA030955 by University Of Colorado Librari, Wiley Online Library on [31.07/2023]. See the Terms and Conditions (https://onlinelibrary.viley.com/doi/10.1029/2022IA03095 by University Of Colorado Library.

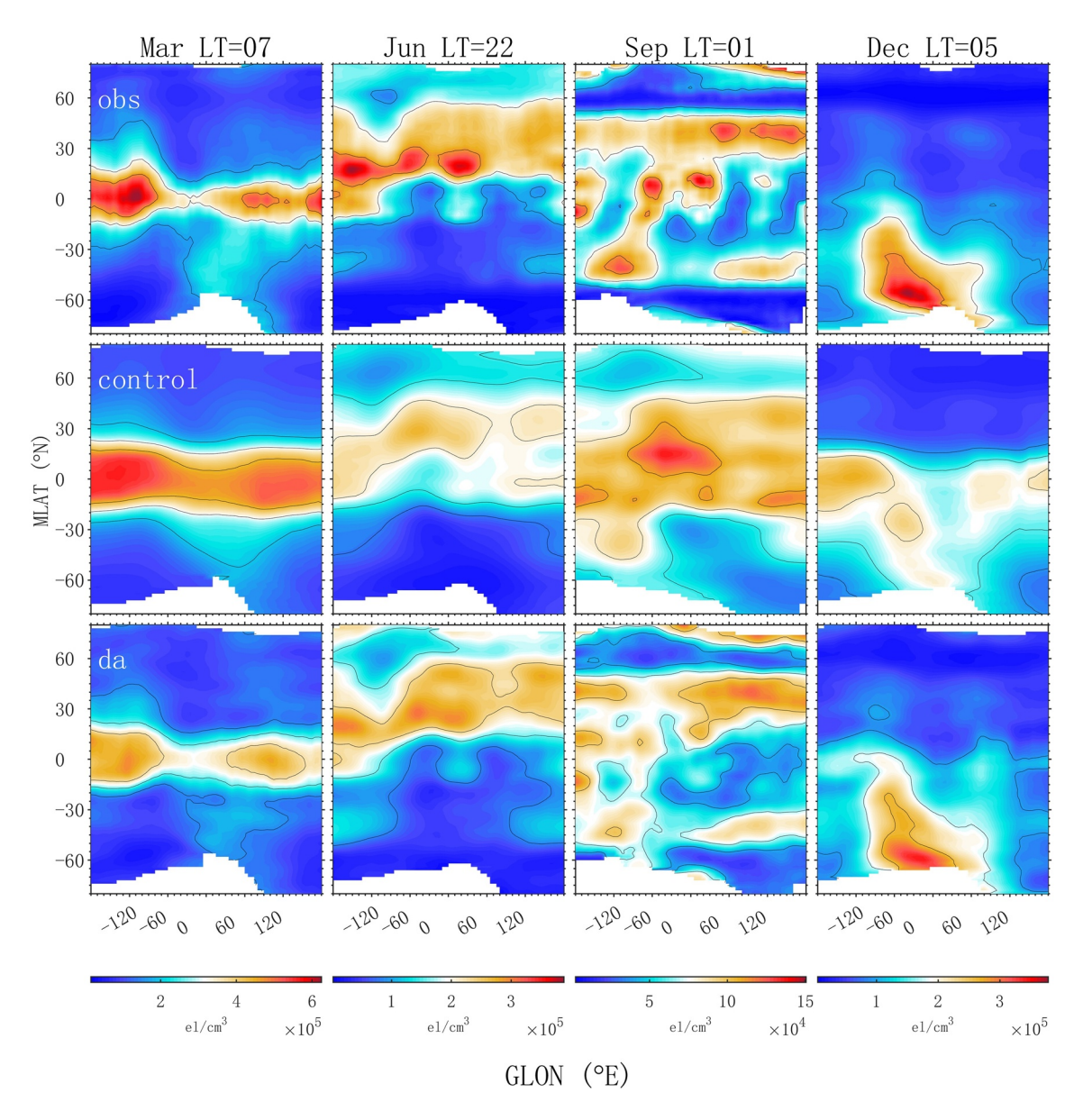


Figure 10. Same as Figure 9, but for nightside electron density comparison.

4. Conclusion

In this paper, the monthly global 3-D ionospheric electron density specification has been performed by solely assimilating COSMIC radio occultation TEC measurements during the geomagnetic quiet days. The selected data assimilation period covers about one solar activity cycle, starting from June of 2006 to the end of December of 2016. The accuracy and reliability of the products of data assimilation results are systematically validated using independent measurements, which generally agree well with the independent observations. In addition, a common ionospheric climatological pattern, including the solar and seasonal variation, annual asymmetry, the Weddell Sea Anomaly, and the longitudinal wave structure, can be well illustrated in the reconstructed 3-D data set. It is a good data set that can be used to study the spatial-temporal variations in ionospheric states from seasons to decades. The current data set can also be used as the background parameters for atmospheric and ionospheric-related scientific research and applications.

HE ET AL. 15 of 17

21699402, 2022, 12, Downloaded from https://agupubs.onlinelibrary.wiley.com/doi/10.1029/2022IA030955 by University Of Colorado Librari, Wiley Online Library on [31/07/2023]. See the Terms and Condition

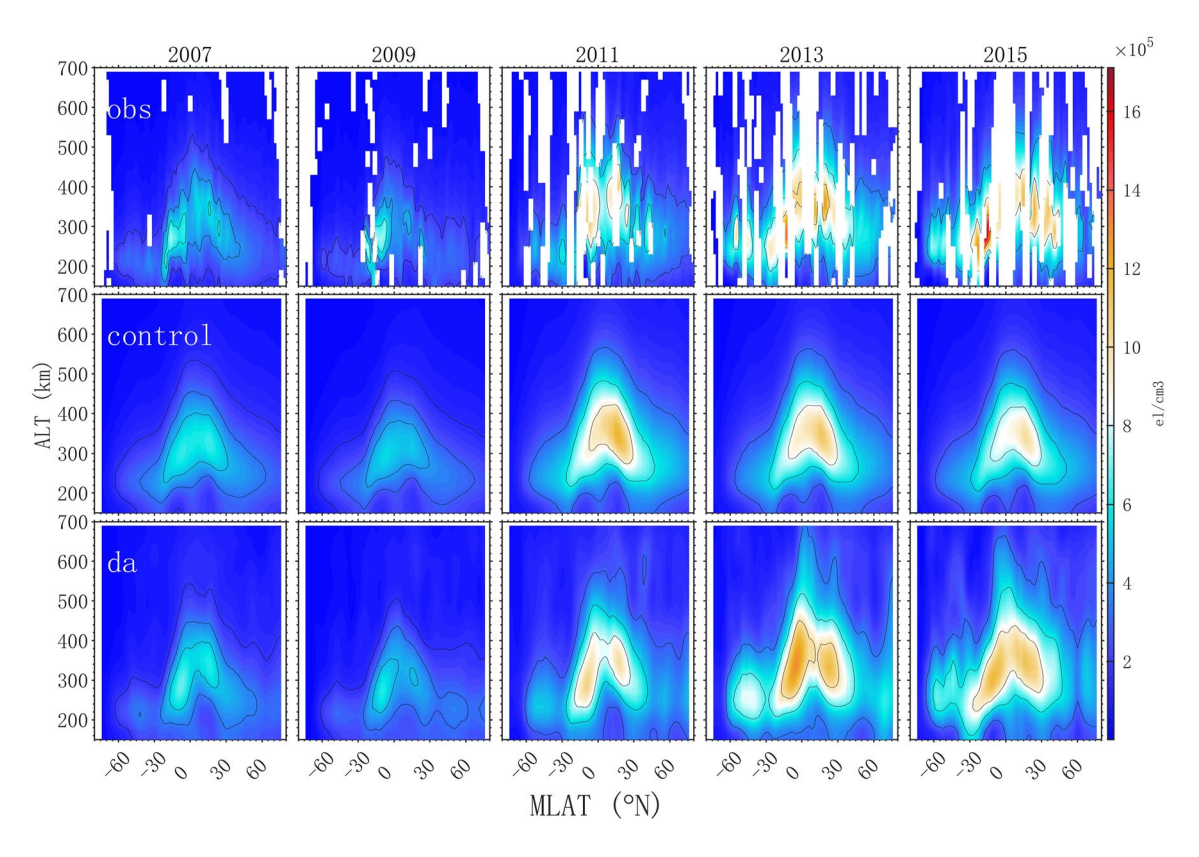


Figure 11. The altitude-magnetic latitude variation of electron density profiles comparison among Constellation Observing System for Meteorology, Ionosphere and Climate electron density profiles measurements, control, and the data assimilation result at 45°E and approximately 1300 local time on June of 2007–2015.

Data Availability Statement

The COSMIC level-1b absolute total electron contents are publicly available at www.cosmic.ucar.edu/what-we-do/cosmic-1/data. The CHAMP level-2 in situ electron density measurements are publicly available from ftp://isdcftp.gfz-potsdam.de/champ. The MIT VTEC observations from the Madrigal Database (cedar.openmadrigal.org). The global ionosonde critical frequency at F2 layer measurements are from the giro.uml.edu. The GRACE occultation TEC data set can be obtained from isdc.gfz-potsdam.de. The monthly global three-dimensional ionospheric electron density data assimilation results presented in this paper has been released and is available for free download from Open Science Framework (http://doi.org/10.17605/OSF.IO/DT6UB).

Acknowledgments

X. Yue, N. Pedatella, and E. Astafyeva acknowledge the ISSI internation team on the ionospheric data assimilation. This work was supported by the Project of Stable Support for Youth Team in Basic Research Field, CAS (YSBR-018), the Chinese Meridian Project, the B-type Strategic Priority Program of the Chinese Academy of Sciences (Grant XDB41000000), the International Partnership Program of Chinese Academy of Sciences (Grant 183311KYSB20200003), the National Natural Science Foundation of China (42104160), and the China Scholarship Council (CSC).

References

Aa, E., Huang, W., Yu, S., Liu, S., Shi, L., Gong, J., et al. (2015). A regional ionospheric TEC mapping technique over China and adjacent areas on the basis of data assimilation. *Journal of Geophysical Research: Space Physics*, 120(6), 5049–5061. https://doi.org/10.1002/2015JA021140
 Aa, E., Zhang, S.-R., Erickson, P. J., Wang, W., Coster, A. J., & Rideout, W. (2022). 3-D regional ionosphere imaging and SED reconstruction with a new TEC-based ionospheric data assimilation system (TIDAS). *Space Weather*, 20(4), e2022SW003055. https://doi.org/10.1029/2022SW003055

Anthes, R. A. (2011). Exploring Earth's atmosphere with radio occultation: Contributions to weather, climate and space weather. Atmospheric Measurement Techniques, 4(6), 1077–1103. https://doi.org/10.5194/amt-4-1077-2011

Bilitza, D. (2001). International reference ionosphere 2000. Radio Science, 36(2), 261–275. https://doi.org/10.1029/2000rs002432

Bust, G. S., Garner, T. W., & Gaussiran, T. L. II. (2004). Ionospheric data assimilation three-dimensional (IDA3D): A global, multisensor, electron density specification algorithm. *Journal of Geophysical Research*, 109(A11), A11312. https://doi.org/10.1029/2003JA010234

Chang, L. C., Lin, C.-H., Yue, J., Liu, J.-Y., & Lin, J.-T. (2013). Stationary planetary wave and nonmigratingtidal signatures in ionospheric wave 3 and wave 4 variations in 2007–2011 FORMOSAT-3/COSMIC observations. *Journal of Geophysical Research: Space Physics*, 118(10), 6651–6665. https://doi.org/10.1002/jgra.50583

Dunn, C., Bertiger, W., Bar-Sever, Y., Desai, S., Haines, B., Kuang, D., et al. (2003). Instrument of GRACE GPS augments gravity measurements. GPS World, 14, 16–29.

Forbes, J. M., Zhang, X., Palo, S., Russell, J., Mertens, C. J., & Mlynczak, M. (2008). Tidal variability in the ionospheric dynamo region. *Journal of Geophysical Research*, 113(A2), A02310. https://doi.org/10.1029/2007JA012737

Galkin, I., Reinisch, B., Huang, X., & Bilitza, D. (2012). Assimilation of GIRO data into a real-time IRI. Radio Science, 47(4), 1–10. https://doi.org/10.1029/2011RS004952

HE ET AL. 16 of 17

- Gardner, L. C., Schunk, R. W., Scherliess, L., Sojka, J. J., & Zhu, L. (2014). Global assimilation of ionospheric measurements-gauss Markov model: Improved specifications with multiple data types. Space Weather, 12, 675–688. https://doi.org/10.1002/2014SW001104
- Gelaro, R., McCarty, W., Suárez, M. J., Todling, R., Molod, A., Takacs, L., et al. (2017). The modern-era retrospective analysis for research and applications, version 2 (MERRA-2). *Journal of Climate*, 30(14), 5419–5454. https://doi.org/10.1175/JCLI-D-16-0758.1
- He, J., Yue, X., Le, H., Ren, Z., & Ding, F. (2022). High-resolution and accurate low-latitude gridded electron density generation and evaluation. Journal of Geophysical Research: Space Physics, 127(4), e2021JA030192. https://doi.org/10.1029/2021JA030192
- Hersbach, H., Bell, B., Berrisford, P., Hirahara, S., Horányi, A., Muñoz-Sabater, J., et al. (2020). The ERA5 global reanalysis. *Quarterly Journal of the Royal Meteorological Society*, 146(730), 1999–2049. https://doi.org/10.1002/qj.3803
- Hoffmann, L., Günther, G., Li, D., Stein, O., Wu, X., Griessbach, S., et al. (2019). From ERA-interim to ERA5: The considerable impact of ECMWF's next-generation reanalysis on Lagrangian transport simulations. Atmospheric Chemistry and Physics, 19(5), 3097–3124. https://doi.org/10.5194/acp-19-3097-2019
- Hsu, C.-T., Matsuo, T., & Liu, J.-Y. (2018). Impact of assimilating the FORMOSAT-3/COSMIC and FORMOSAT-7/COSMIC-2 RO data on the midlatitude and low-latitude ionospheric specification. Earth and Space Science, 5(12), 875–890. https://doi.org/10.1029/2018EA000447
- Huang, H., Lu, X., Liu, L., Wang, W., & Li, Q. (2018). Transition of interhemispheric asymmetry of equatorial ionization anomaly during solstices. *Journal of Geophysical Research: Space Physics*, 123, 10283–10300. https://doi.org/10.1029/2018JA026055
- Jakowski, N., Béniguel, Y., De Franceschi, G., Pajares, M. H., Jacobsen, K. S., Stanislawska, I., et al. (2012). Monitoring, tracking and fore-casting ionospheric perturbations using GNSS techniques. *Journal of Space Weather and Space Climate*, 2, A22. https://doi.org/10.1051/swsc/2012022
- Le, H., Han, T., Li, Q., Liu, L., Chen, Y., & Zhang, H. (2022). A new global ionospheric electron density model based on Grid Modeling method. Space Weather, 20(6), e2021SW002992. https://doi.org/10.1029/2021SW002992
- Luan, X., Wang, P., Dou, X., & Liu, Y. C. M. (2015). Interhemispheric asymmetry of the equatorial ionization anomaly in solstices observed by cosmic during 2007–2012. *Journal of Geophysical Research: Space Physics*, 120(4), 3059–3073. https://doi.org/10.1002/2014JA020820
- Mannucci, A., Tsurutani, B., Iijima, B., Komjathy, A., Saito, A., Gonzalez, W., et al. (2005). Dayside global ionospheric response to the major interplanetary events of October 29–30, 2003 "Halloween Storms". Geophysical Research Letters, 32(12), L12S02. https://doi. org/10.1029/2004GL021467
- Matsuo, T., & Araujo-Pradere, E. (2011). A. Role of thermosphere-ionosphere coupling in a global ionospheric specification. *Radio Science*, 46(6), 1–7. https://doi.org/10.1029/2010RS004576
- McNamara, L., Cooke, D., Valladares, C., & Reinisch, B. (2007). Comparison of CHAMP and Digisonde plasma frequencies at Jicamarca, Peru. Radio Science, 42(2), 1–14. https://doi.org/10.1029/2006RS003491
- Molod, A., Takacs, L., Suarez, M., & Bacmeister, J. (2015). Development of the GEOS-5 atmospheric general circulation model: Evolution from MERRA to MERRA2. Geoscientific Model Development, 8(5), 1339–1356. https://doi.org/10.5194/gmd-8-1339-2015
- Nava, B., Coisson, P., & Radicella, S. (2008). A new version of the NeQuick ionosphere electron density model. *Journal of Atmospheric and Solar-Terrestrial Physics*, 70(15), 1856–1862. https://doi.org/10.1016/j.jastp.2008.01.015
- Pedatella, N. M., Zakharenkova, I., Braun, J. J., Cherniak, I., Hunt, D., Schreiner, W. S., et al. (2021). Processing and validation of FORMOSAT-7/COSMIC-2 GPS total electron content observations. *Radio Science*, 56(8), e2021RS007267. https://doi.org/10.1029/2021RS007267
- Reinisch, B. W., & Galkin, I. A. (2011). Global ionospheric radio observatory (GIRO). Earth Planets and Space, 63(4), 377–381. https://doi.org/10.5047/eps.2011.03.001
- Rideout, W., & Coster, A. (2006). Automated GPS processing for global total electron content data. GPS Solutions, 10(3), 219–228. https://doi.org/10.1007/S10291-006-0029-5
- Rocken, C., Ying-Hwa, K., Schreiner, W. S., Hunt, D., Sokolovskiy, S., & McCormick, C. (2000). COSMIC system description. *Terrestrial, Atmospheric and Oceanic Sciences*, 11(1), 21–52. https://doi.org/10.3319/tao.2000.11.1.21(cosmic)
- Schunk, R. W., Scherliess, L., Sojika, J. J., Thompson, D. C., Anderson, D. N., Codrescu, M., et al. (2004). Global assimilation of ionospheric measurements (GAIM). Radio Science, 39(1), RS1S02. https://doi.org/10.1029/2002RS002794
- Tapley, B. D., Bettadpur, S., Watkins, M., & Reigber, C. (2004). The gravity recovery and climate experiment: Mission overview and early results. Geophysical Research Letters, 31(9), L09607. https://doi.org/10.1029/2004GL019920
- Wan, W., Liu, L., Pi, X., Zhang, M.-L., Ning, B., Xiong, J., & Ding, F. (2008). Wavenumber-4 patterns of the total electron content over the low latitude ionosphere. *Geophysical Research Letters*, 35(12), L12104. https://doi.org/10.1029/2008GL033755
- Wang, C., Hajj, G., Pi, X., Rosen, I. G., & Wilson, B. (2004). Development of the global assimilative ionospheric model. *Radio Science*, 39(1), RS1S06. https://doi.org/10.1029/2002RS002854
- Yeh, K. C., & Liu, C. H. (1982). Radio wave scintillations in the ionosphere. Proceedings of the IEEE, 70(4), 324–360. https://doi.org/10.1109/proc.1982.12313
- Yue, X., Schreiner, W. S., Hunt, D. C., Rocken, C., & Kuo, Y.-H. (2011). Quantitative evaluation of the low Earth orbit satellite based slant total electron content determination. Space Weather, 9, S09001. https://doi.org/10.1029/2011SW000687
- Yue, X., Schreiner, W. S., Kuo, Y. H., Braun, J. J., Lin, Y., & Wan, W. (2014). Observing system simulation experiment study on imaging the ionosphere by assimilating observations from ground GNSS, LEO-based radio occultation and ocean reflection, and cross link. IEEE Transactions on Geoscience and Remote Sensing, 52(7), 3759–3773. https://doi.org/10.1109/TGRS.2013.2275753
- Yue, X., Schreiner, W. S., Kuo, Y. H., Hunt, D. C., Wang, W., Solomon, S. C., et al. (2012). Global 3-D ionospheric electron density reanalysis based on multisource data assimilation. *Journal of Geophysical Research*, 117(A9), A09325. https://doi.org/10.1029/2012JA017968
- Yue, X., Schreiner, W. S., Lei, J., Sokolovskiy, S. V., Rocken, C., Hunt, D. C., & Kuo, Y.-H. (2010). Error analysis of Abel retrieved electron density profiles from radio occultation measurements. Annals of Geophysics, 28(1), 217–222. https://doi.org/10.5194/angeo-28-217-2010
- Zhang, S.-R., & Holt, J. M. (2004). Ionospheric plasma temperatures during 1976–2001 over Millstone Hill. Advances in Space Research, 33(6), 963–969. https://doi.org/10.1016/j.asr.2003.07.012

HE ET AL. 17 of 17